Research Article | Vol. 24, No. 14 | 11 Jul 2016 | OPTICS EXPRESS A1158

Optics EXPRESS

Exploration of external light trapping for photovoltaic modules

LOURENS VAN DIJK,[1,*] JORIK VAN DE GROEP,[2] MARCEL DI VECE,[1] AND RUUD E. I. SCHROPP[3]

[1]*Utrecht University, Nanophotonics - Physics of Devices, Debye Institute for Nanomaterials Science, High Tech Campus, Building 21, 5656 AE Eindhoven, The Netherlands*
[2]*FOM Institute AMOLF, Science Park Amsterdam 104, 1098 XG Amsterdam, The Netherlands*
[3]*Eindhoven University of Technology (TU/e), Department of Applied Physics, Plasma and Materials Processing, 5600 MB Eindhoven, The Netherlands*
[*]*l.vandijk@uu.nl*

Abstract: The reflection of incident sunlight by photovoltaic modules prevents them from reaching their theoretical energy conversion limit. We explore the effectiveness of a universal external light trap that can tackle this reflection loss. A unique feature of external light traps is their capability to simultaneously recycle various broadband sources of reflection on the module level, such as the reflection from the metal front grid, the front interfaces, the reflective backside of the cell, and the white back sheet. The reflected light is recycled in the space between the solar cell and a mirror above the solar cell. A concentrator funnels the light into this cage through a small aperture in the mirror. As a proof-of-principle experiment, a significant reflectance reduction of a bare crystalline silicon (c-Si) photodiode is demonstrated. In contrast to conventional light trapping methods, external light trapping does not induce any damage to the active solar cell material. Moreover, this is a universally applicable technology that enables the use of thin and planar solar cells of superior electrical quality that were so far hindered by limited optical absorption. We considered several trap designs and identified fabrication issues. A series of prototype millimeter-scale external metal light traps were milled and applied on an untextured c-Si photodiode, which is used as a model for future thin solar cells. We determined the concentrator transmittance and analyzed the effect of both the concentration factor and cage height on the absorptance and spatial intensity distribution on the surface of the solar cell. This relatively simple and comprehensive light management solution can be a promising candidate for highly efficient solar modules using thin c-Si solar cells.

© 2016 Optical Society of America

OCIS codes: (350.6050) Solar energy; (080.4298) Nonimaging optics; (080.3630) Lenses; (040.5350) Photovoltaic.

References and links

1. T. Mishima, M. Taguchi, H. Sakata, and E. Maruyama, "Development status of high-efficiency HIT solar cells," Sol. Energ. Mat. Sol. C. **95**, 18–21 (2011).
2. S. C. Baker-Finch, "Rules and tools for understanding, modelling and designing textured silicon solar cells," Thesis Australian National University (2012).
3. A. Luque and S. Hegedus, *Handbook of Photovoltaic Science and Engineering* (John Wiley & Sons, 2011).
4. S. C. Baker-Finch and K. R. McIntosh, "Reflection of normally incident light from silicon solar cells with pyramidal texture," Prog. Photovolt. Res. Appl. **19**, 406–416 (2011).
5. D. Macdonald, A. Cuevas, M. J. Kerr, C. Samundsett, D. Ruby, S. Winderbaum, and A. Leo, "Texturing industrial multicrystalline silicon solar cells," Sol. Energy **76**, 277–283 (2004).
6. R. J. Beal, B. G. Potter, and J. H. Simmons, "Angle of incidence effects on external quantum efficiency in multicrystalline silicon photovoltaics," IEEE J. Photovolt. **4**, 1459–1464 (2014).
7. H. Savin, P. Repo, G. von Gastrow, P. Ortega, E. Calle, M. Garín, and R. Alcubilla, "Black silicon solar cells with interdigitated back-contacts achieve 22.1% efficiency," Nat. Nanotechnol. **10**, 624–628 (2015).
8. P. Campbell and M. A. Green, "The limiting efficiency of silicon solar cells under concentrated sunlight," IEEE T. Electron. Dev. **33**, 234–239 (1986).
9. A. Gabor, "Cell-to-module gains and losses in crystalline silicon pv, gabor photovoltaics consulting," July 10, 2013 Intersolar NA.
10. G. Peharz, W. Nemitz, V. Schmidt, S. Schweitzer, W. Mühleisen, and C. Hirschl, "Investigations on the photon-recycling properties of different back-sheets," in Proceedings of EUPVSEC, (2014), pp. 3115-3118.

#261036 http://dx.doi.org/10.1364/OE.24.0A1158
Journal © 2016 Received 21 Mar 2016; revised 19 May 2016; accepted 21 May 2016; published 29 Jun 2016

Optics EXPRESS

11. "Pvlighthouse - tracey," www.pvlighthouse.com.au.
12. K. X. Wang, Z. Yu, V. Liu, Y. Cui, and S. Fan, "Absorption enhancement in ultrathin crystalline silicon solar cells with antireflection and light-trapping nanocone gratings," Nano Lett. **12**, 1616–1619 (2012).
13. A. Richter, S. W. Glunz, F. Werner, J. Schmidt, and A. Cuevas, "Improved quantitative description of auger recombination in crystalline silicon," Phys. Rev. B **86**, 165202 (2012).
14. M. Kerr, J. Schmidt, A. Cuevas, and J. Bultman, "Surface recombination velocity of phosphorus-diffused silicon solar cell emitters passivated with plasma enhanced chemical vapor deposited silicon nitride and thermal silicon oxide," J. Appl. Phys. **89**, 3821–3826 (2001).
15. H. Jin and K. Weber, "Relationship between interface defect density and surface recombination velocity in (111) and (100) silicon/silicon oxide structure," in Proceedings of EUPVSEC, (2008), pp. 244-247.
16. K. Xiong, S. Lu, D. Jiang, J. Dong, and H. Yang, "Effective recombination velocity of textured surfaces," Appl. Phys. Lett. **96**, 193107 (2010).
17. M. Green, "Limits on the open-circuit voltage and efficiency of silicon solar cells imposed by intrinsic auger processes," IEEE Trans. Electron. Dev. **31**, 671–678 (1984).
18. E. D. Kosten, B. K. Newman, J. V. Lloyd, A. Polman, and H. Atwater, "Limiting light escape angle in silicon photovoltaics: ideal and realistic cells," IEEE J. Photovolt. **5**, 61–69 (2015).
19. Consortium of several companies and research institutes, "International technology roadmap for photovoltaic (itrpv)", www.itrpv.net.
20. M. F. Schumann, S. Wiesendanger, J. C. Goldschmidt, B. Bläsi, K. Bittkau, U. W. Paetzold, A. Sprafke, R. B. Wehrspohn, C. Rockstuhl, and M. Wegener, "Cloaked contact grids on solar cells by coordinate transformations: designs and prototypes," Optica **2**, 850–853 (2015).
21. P. Verlinden, R. Swanson, and R. Crane, "7000 high-eficiency cells for a dream," Prog. Photovolt. Res. Appl. **2**, 143–152 (1994).
22. M. Peters, J. C. Goldschmidt, T. Kirchartz, and B. Bläsi, "The photonic light trap - improved light trapping in solar cells by angularly selective filters," Sol. Energ. Mat. Sol. C. **93**, 1721–1727 (2009).
23. C. Ulbrich, M. Peters, B. Bläsi, T. Kirchartz, A. Gerber, and U. Rau, "Enhanced light trapping in thin-film solar cells by a directionally selective filter," Opt. Express **18**, A133–A138 (2010).
24. O. Höhn, T. Kraus, G. Bauhuis, U. T. Schwarz, and B. Bläsi, "Maximal power output by solar cells with angular confinement," Opt. Express **22**, A715–A722 (2014).
25. E. D. Kosten, B. M. Kayes, and H. A. Atwater, "Experimental demonstration of enhanced photon recycling in angle-restricted gaas solar cells," Energ. Environ. Sci. **7**, 1907–1912 (2014).
26. R. A. Sinton and R. M. Swanson, "Increased photogeneration in thin silicon concentrator solar cells," Electron Devic. Lett., IEEE **8**, 547–549 (1987).
27. A. Luque and J. C. Miñano, "Optical aspects in photovoltaic energy conversion," Sol. Cells **31**, 237–258 (1991).
28. J. M. Gordon, D. Feuermann, and H. Mashaal, "Micro-optical designs for angular confinement in solar cells," J. Photon. Energy **5**, 055599–055599 (2015).
29. A. Braun, E. A. Katz, D. Feuermann, B. M. Kayes, and J. M. Gordon, "Photovoltaic performance enhancement by external recycling of photon emission," Energ. Environ. Sci. **6**, 1499–1503 (2013).
30. L. A. Weinstein, W.-C. Hsu, S. Yerci, S. V. Boriskina, and G. Chen, "Enhanced absorption of thin-film photovoltaic cells using an optical cavity," J. Opt. **17**, 055901 (2015).
31. L. van Dijk, E. P. Marcus, A. J. Oostra, R. E. I. Schropp, and M. Di Vece, "3d-printed concentrator arrays for external light trapping on thin film solar cells," Sol. Energ. Mat. Sol. C. **139**, 19–26 (2015).
32. L. van Dijk, U. W. Paetzold, G. A. Blab, R. E. I. Schropp, and M. Di Vece, "3D-printed external light trap for solar cells," Prog. Photovolt. Res. Appl. **24**, 623–633 (2016).
33. "Edmund optics, item nr. 63-229 (CPC)," www.edmundoptics.com.
34. I. Papakonstantinou and C. Tummeltshammer, "Fundamental limits of concentration in luminescent solar concentrators revised: the effect of reabsorption and nonunity quantum yield," Optica **2**, 841–849 (2015).
35. G. E. Arnaoutakis, J. Marques-Hueso, A. Ivaturi, S. Fischer, J. C. Goldschmidt, K. W. Krämer, and B. S. Richards, "Enhanced energy conversion of up-conversion solar cells by the integration of compound parabolic concentrating optics," Sol. Energ. Mat. Sol. C. **140**, 217–223 (2015).
36. J. H. Atwater, P. Spinelli, E. Kosten, J. Parsons, C. van Lare, J. van de Groep, J. Garcia de Abajo, A. Polman, and H. A. Atwater, "Microphotonic parabolic light directors fabricated by two-photon lithography," Appl. Phys. Lett. **99**, 151113–151113 (2011).
37. J. Miñano, A. Luque, and I. Tobias, "Light-confining cavities for photovoltaic applications based on the angular-spatial limitation of the escaping beam," Appl. Opt. **31**, 3114–3122 (1992).
38. "Hamamatsu," www.hamamatsu.com.
39. U. Rau, U. W. Paetzold, and T. Kirchartz, "Thermodynamics of light management in photovoltaic devices," Phys. Rev. B **90**, 035211 (2014).
40. M. Planck, "The theory of heat radiation (translation)," Masius, P. Blackiston's Son & Co, Philadelphia (1914).
41. P. Würfel and U. Würfel, *Physics of Solar Cells: From Basic Principles to Advanced Concepts* (John Wiley & Sons, 2009).
42. R. Winston, J. Miñano, and P. Benítez, *Nonimaging Optics*, Electronics & Electrical (Elsevier Academic, 2005).
43. A. Luque, G. Sala, and J. Arboiro, "Electric and thermal model for non-uniformly illuminated concentration cells,"

Optics EXPRESS

Sol. Energ. Mat. Sol. C. **51**, 269–290 (1998).
44. M. Tormen, O. Inganäs, K. Tvingstedt, and S. Zilio, "Photovoltaic device with enhanced light harvesting," (2010). US Patent App. 12/601,798.
45. K. Lee, J. Lee, B. A. Mazor, and S. R. Forrest, "Transforming the cost of solar-to-electrical energy conversion: Integrating thin-film GaAs solar cells with non-tracking mini-concentrators," Light Sci. Appl. **4**, e288 (2015).
46. J. S. Price, X. Sheng, B. M. Meulblok, J. A. Rogers, and N. C. Giebink, "Wide-angle planar microtracking for quasi-static microcell concentrating photovoltaics," Nat. commun. **6**, 6223 (2015).

1. Introduction

All solar cell technologies exhibit optical reflection losses that limit the power conversion efficiency. For example, industrial crystalline silicon (c-Si) based solar modules are hindered by reflection from the metal front grid (fingers and busbars), front interfaces, and incomplete fill factor of the module area ("optically dead area"). Long wavelengths are reflected out of the module due imperfect absorption. Highly efficient solar modules thus require a general solution that simultaneously recycles the broadband light from these four reflection sources on the module level.

The optical loss due to the surface coverage by the grid of industrial c-Si modules is typically 5-10% [1–3]. The optical absorption of c-Si cells is generally enhanced by texturing the surface, which results in both improved light incoupling and internal light trapping. However, even for textured cells, the reflection at normal incidence from the front interfaces (air-glass-ethylene-vinyl acetate (EVA)-cell) ranges from 5.5%-6% for encapsulated textured mono-c-Si (mono-Si) modules [4]; ∼613% for multi-c-Si (multi-Si) modules [5, 6]; and less than 6% for heterojunction (HIT^{TM}) cells [1]. For larger angles of incidence, the reflectance is significantly larger [6, 7]. Around 2-6% percent of the light escapes the cell due to imperfect absorption [1, 8], mainly caused by wavelengths near the band-edge. Finally, ∼2-10% of the total module area is covered by an inactive back-sheet [2, 9]. For white back-sheets, around 80% of the reflected light escapes from the module [10]. Although the sum of these four reflection losses varies by manufacturer, typically more than 13% of the potential short circuit current is lost due to reflection [11].

Generally, the optical absorptance of a cell is enhanced by increasing the cell thickness and by texturization of the front surface [12]. However, increasing the thickness results in an increase of Auger and Shockley-Read-Hall recombination [13]. Texturing results in a larger surface area and thereby higher surface recombination [14–16]. The probability for charge carriers to recombine can therefore be reduced by using a thin and planar c-Si solar cell that benefit from a high open circuit voltage (V_{oc}). It has been shown that thin c-Si cells with angular restriction can have a V_{oc} close to 800 mV [17, 18]. Over the past decades, the thickness of commercial c-Si solar cells has been reduced from roughly 300 μm to 175 μm. It is expected that the average wafer thickness will drop further to 100 μm in 2024 [19]. This trend is driven by significant advantages of thin cells, such as their low material cost, reduced weight, and low bulk recombination. Moreover, once the cell thickness drops below 50 μm, texturing cannot easily be applied as the texture dimensions become similar to the cell thickness. Companies like 1366Technologies and NexWafe are producing such thin wafers by kerfless methods. Due to their thin absorber, these cells require even more efficient light trapping methods than today's available options.

There exist many light trapping solutions that resolve one of the four aforementioned reflection losses. For example, prismatic covers, SmartWire, contact cloaking [20], and interdigitated back contact technologies [21] have been used to reduce or eliminate reflection loss from the front contacts. One can improve the absorption within the c-Si by limiting the escape probability of photons inside the cell using angular restriction. This restriction can be realized by multilayer stacks and Rugate filters [22–25]. However, these solutions have in common that they only resolve one of the four indicated reflection sources and/or are limited to narrowband improvements as a result of their resonant nature. Moreover, many of these solutions suffer from significant parasitic absorptance.

Optics EXPRESS

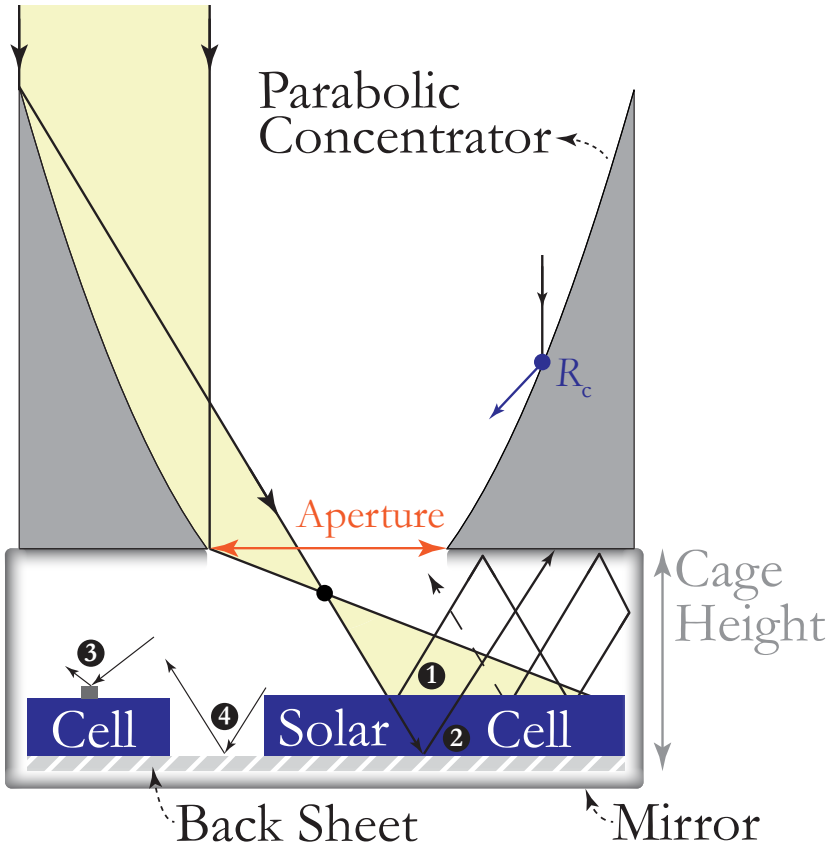

Fig. 1. Illustration of a cross section of an external light trap on top of a specularly reflective solar cell. Light is focused through an aperture and is trapped within a cage. The reflectivity of the concentrator (R_c) and that of the cage are important parameters of the light trap. The cage height determines the optical path within the cage and the intensity distribution on the solar cell. Light reflecting from the front interfaces (182), back interfaces (183), metal grid (184), and white back sheet (185) is recycled.

Here, we explore the effectiveness of a universal external light trap for solar modules, and in particular modules with thin c-Si solar cells. The key concept of external light trapping is illustrated in Fig. 1. Incident sunlight is focused through a small aperture by a parabolic mirror. The light enters a cage and diverges before it reaches the cell. Most of the light that reflects from the solar module is retro-reflected and recycled in this optical cavity. External light trapping addresses the four indicated reflection losses at once. At the same time, the trap enables the use of thinner cells with higher power conversion efficiency [8, 26–28] and can supplement or take over the anti-reflection role of the front texture and enable planar front textures. As the external light trap facilitates improved in-coupling of light, it becomes interesting to have a planar front surface and only texture the backside of the solar cell to scatter the light for internal light trapping. This enables less surface recombination and thus higher cell efficiency. Texturing the cell for internal light trapping has slight drawbacks and becomes increasingly difficult as wafers get thinner [14–16]. Interestingly, the external light trapping concept decouples the optical properties from the electronic properties. Thereby, it is able to improve the absorptance without inducing any damage to the active cell material.

The conceptual idea of external light trapping and angular restriction recently draw attention

Optics EXPRESS

due to its potential for efficiency enhancement [28–32]. As the trap is universally applicable, it is of special interest for multi-Si, because multi–Si cannot be textured as effective as mono-c-Si [3]. The external light trap works over the full solar spectrum (if the concentrator has excellent transmittance) and can be integrated industrially at low costs. Moreover, by external light trapping one can surpass the $4n^2$ path length enhancement limit as the trap acts as a multiplier of the internal path length enhancement [31]. External light trapping is based on relatively simple reflective geometric optics and thereby virtually wavelength independent. Furthermore, external light trapping could be of interest for a wide variety of solar applications, such as luminescent solar concentrators [34], up-conversion [35], and thin-film solar cells which have low-index absorber layers (e.g. Perovskites) for which internal light trapping is less effective [31].

We stress that the use of a concentrator in an external light trap differs from its use in concentrated photovoltaics (CPV). In CPV the photon flux is increased to allow a reduction of the cell area, while for external light trapping the goal is to improve the cell absorptance. Interestingly, CPV and external light trapping light can be combined by making the cell area larger than the aperture area but smaller than the concentrator opening to realize both concentration and light trapping [32].

Recently, we demonstrated the effectiveness of 3D-printed external light traps for thin film nanocrystalline Si and organic solar cells [31, 32]. In this work, we fabricated several millimeter-scale concentrators using an industrial milling process. This method offers higher contour accuracy and the strong metal parts can be used as a mold for cheap, large area fabrication of thermoplastic concentrators. Similar designs have been fabricated on micro-scale [36], but for commercial application a millimeter scale design is expected to have lower fabrication costs and to yield higher performance [31]. We analyze several fabrication aspects that determine the transmittance of the concentrator of the external light trap.

As a proof-of-principle experiment, we use a c-Si photodiode as a simple model for thin and planar c-Si solar cell. We demonstrate a 64% reflectance reduction of a bare c-Si solar photodiode due to an external light trap. The performance of the parabolic concentrator is analyzed by comparing the theoretical and experimental polarization dependent transmittance maps. Previous optical analytic external light trapping models where based on complete randomization of light within the cage [26, 32, 37]. We demonstrate the accuracy of this analytic model for our external light trap by ray tracing. Also, we determine the effect of both the geometric concentration factor and cage height on the total cell absorptance and spatial intensity distribution on the cell. We show that the use of a tall cage results in homogeneous cell illumination except for the center of the solar cell.

2. Materials and methods

We fabricated concentrators with different concentration factors (3–9×) and cages with different heights (1–4 mm) out of aluminum using an industrial CNC milling machine. To improve the reflectivity, the parts were thoroughly cleaned and sputter-coated with a 400 nm thick layer of silver. Figure 2 shows three milled parabolic concentrators with different geometric concentration factor (C) and three cages with a different height.

Fabrication. The concentrators and light cages are milled out of an aluminum rod by a milling cutter machine (Fehlmann P90). The milling head is shown in Fig. 3(a). A cooling liquid (a mixture of water and oil) is used to cool and lubricate the workpiece, see Fig. 3(b). The liquid also helps to reduce the stickiness and to get rid of the aluminum chips that are released during the milling. The fabrication involves several steps. First a roughing cut is performed to make the rough basic shape of the concentrator and to remove most of the material. Next, a finishing cut is performed using a smaller ball mill. The workpiece (which will become the concentrator) slowly rotates below the fast rotating ball mill, while the ball mill translates radially inward and downwards along the intended surface shape. If the ball mill would move layer-by-layer on

Optics EXPRESS

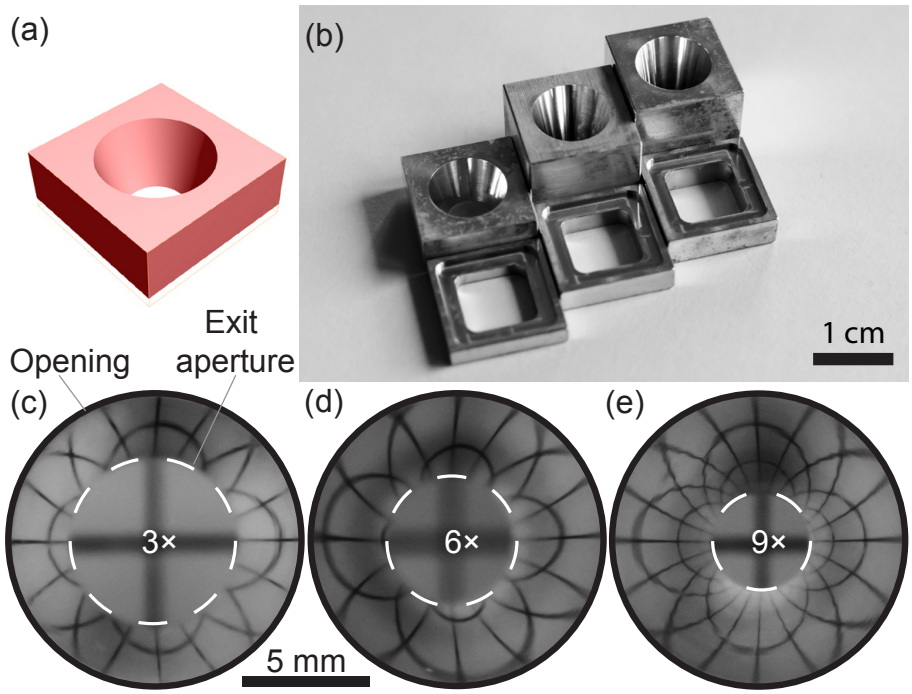

Fig. 2. **(a)** Design of the 3× concentrator. **(b)** Photo of the milled concentrators and the cages. The milled concentrators have a concentration factor of 3×, 6×, and 9×. The cages make a vertical spacing between the cell and the reflective bottom of the concentrator of 2, 3, and 4 mm. (**c-e**) Photos of the top view of the concentrators with different concentration factor: **(c)** $C = 3\times$, **(d)** $C = 6\times$, and **(e)** $C = 9\times$. The concentrators are placed 3 cm from a sheet of squared graph paper. The center (in white dashed ring) shows a direct view of the squared graph paper (out of focus) through the aperture. Outside the center, a distorted image is formed of the straight lines of the graph paper due to the concentrator curvature. The camera is focused on the concentrator surface.

circular tracks, there would be some places with a discrete vertical step. This leaves an unwanted artifact in the workpiece. To prevent these discrete steps, the milling cutter moves along a spiral track, which can be realized by tilting the concentrator by ∼2 degrees.

Polishing. The milling process leaves small grooves in the surface of the concentrator. These grooves reduce the reflectance and thus the performance of the concentrator. Scratches can lead to elevated absorptance of the metal surface and it can also reflect or scatter the light in unintended directions. By polishing, a surface the peaks on the surface are flattened by making new, but smaller scratches. In general, the polishing of hollow objects is much more difficult than convex shapes as one can not use conventional lapping techniques for hollow surfaces. To smoothen the hollow surface, we placed the work piece in a lathe. While the work piece rotated we inserted a cotton swab and polishing abrasives to reduce the surface roughness. To remove all residuals of the milling process, we did extensive cleaning with soap followed by ultrasonic cleaning in anisole (8 min) and ethanol (60 min). To obtain smoother surfaces one could consider the use of an intermediate overcoat layer to smoothen the surface. Many paints produce a very smooth surface due to surface tension [32]. The flat bottom of the concentrator was manually polished by lapping on a flat plate. The grain size of the lapping powder was reduced in steps from 5 μm to 0.5 μm.

Solar cell specifications. We use a common c-Si photodiode as a model system to show

Optics EXPRESS

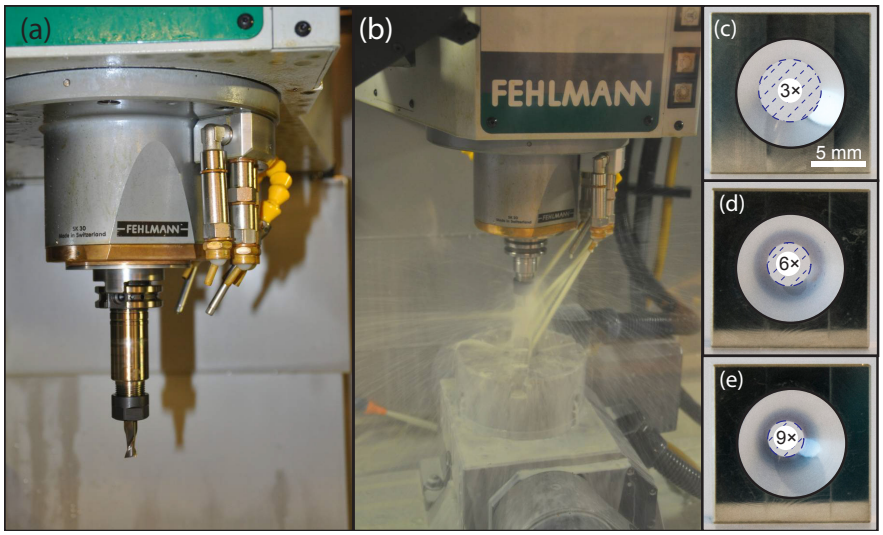

Fig. 3. (**a**) Close-up of the milling head inside the milling cutter machine. (**b**) Milling process of the external light trap. The aluminum rod that will become the concentrator is fixed in the setup. Various bits are used for the different fabrication stages of the concentrator. A beam of cooling liquid is used to carry away heat generated during the milling and to remove the released metal chips during the milling. (**c-e**) Top view of the concentrators with different concentration factor (C=3-9×).

the potential of this concept for thin c-Si solar cells. The 1 cm^2 c-Si Hamamatsu photodiode (S1337-1010BQ [38]) serves as a model system to study the effect of concentration factor and cage height. The photodiode has an untextured front surface, a thickness of 300 μm, a quartz window layer, and does not have an anti-reflection coating (ARC). The reflection of this c-Si photodiode is higher than that of solar modules, but in the near-infrared it resembles that of a thin c-Si cell with an ARC. As the external light trap is indifferent with respect to the origin of the reflected light, the photodiode is a reasonable model for a module with thin c-Si solar cells.

By demonstrating light trapping of light reflecting at the front side of the cell, we simultaneously demonstrate the potential for trapping of light reflected at the backside of a (thin) c-Si solar cell. Although the wavelength-dependent reflectance of a thin cell is different from that of the cell used in this experiment, the optics involved is equivalent. The photodiode does not have an electrical front grid; the current is collected at the edge of the front surface. It is challenging to use a front-contacted solar cell, as this complicates the experimental measurement. For example, the electrical probes interfere (e.g. absorb) with the external light trap. The use of the indicated photodiode circumvents this problem as the photodiode is contacted outside the optically sensitive area.

Material costs. Various options are available for the type of concentrator, e.g. metalized hollow parabolic concentrators and dielectric CPCs [33]. The additional silver increases the total module cost; for the spot price of silver (∼560 \$/kg) the material cost for a 400 nm thick silver layer is around 2.35 $\$/m^2$. Note that thin inner coatings of the cage do not need to be specularly reflecting and can be replaced by a white diffuse reflector, rather than Ag. The polymer cost of an injection molded concentrator array made of Acrylonitrile Butadiene Styrene (ABS) is in the order of several $\$/m^2$. On the other hand, the external light trap enables the use of thinner cells having lower material cost. In the end, these two factors and the enhanced efficiency determine the effect on the cost ($\$/W_p$) of the module. However, this is not the only important economical metric; the module efficiency and its aesthetic appearance are also important factors for the price

Optics EXPRESS

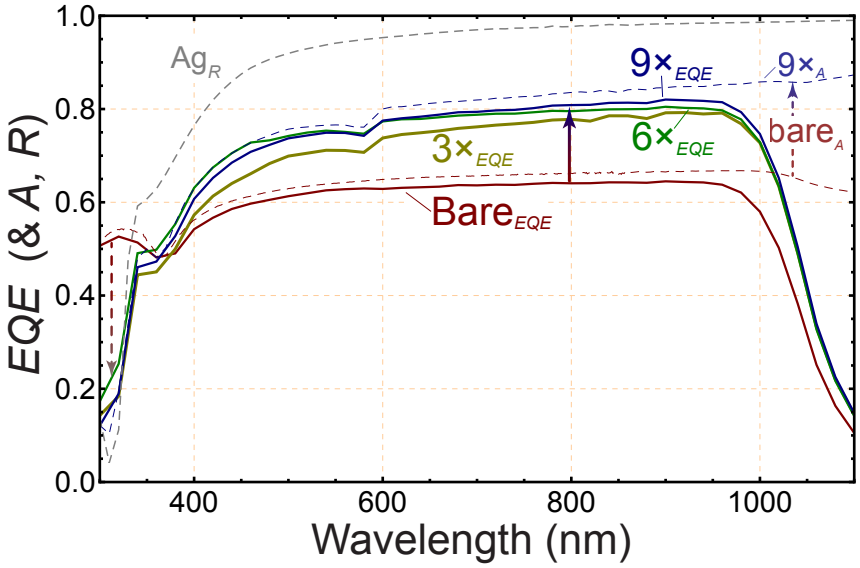

Fig. 4. Plot of the EQE for various trap configurations. The red solid line shows the EQE of the bare, flat, and untextured c-Si solar cell. The yellow, green, and blue solid line are the best measured EQE of the c-Si cell with a cage height of 4 mm external light traps with respectively C=3, 6, and 9×. The red dashed line shows the measured absorptance of the bare cell (bare$_A$). The blue dashed line shows the calculated absorptance of the cell with the 9× concentrator applied. The gray dashed line is the measured reflectance of polished silver coated aluminum.

that customers are willing to pay.

Setup. An important metric of the solar cell with and without external light trap is the (wavelength dependent) ratio between the number of collected electrons and incident photons. The EQE was determined using a commercial setup from OptoSolar. Monochromatic light was selected from a broadband light source (Xenon arc lamp) combined with a grating based monochromator and a color filter wheel. The spectral bandwidth of beam is ∼10–15 nm. The spectral intensity of the beam is smaller than that of the sun (roughly one order of magnitude smaller per bandwidth interval). The response of the photodiode is linear in this intensity regime. The results obtained for a low-intensity beam give a good approximation of the response at 1 sun irradiance. The incident (collimated) beam has a diameter of ∼2.5 mm. As the EQE describes a ratio between collected electrons and incident photons, the EQE is an area independent quantity. Therefore, the diameter of the beam does not affect the measured EQE.

3. Results and discussion

***EQE* for several concentration factors**. The spectral response of the cell was measured for different trap configurations. Figure 4 shows the absorptance ($A = 1 - R$, dashed) and the external quantum efficiency (EQE, solid) of the bare solar cell and of the cell with light traps with different concentration factors (3–9×).

Overall, the bare cell has an EQE (bare$_{EQE}$) of ∼58-64%, and an absorptance (bare$_A$) of ∼60-66%. The dip in the absorptance of the bare cell around ∼360 nm is a result of strong reflection from the c-Si front interface. For wavelengths longer than 950 nm, bare$_{EQE}$ drops significantly as there is only little absorption in the c-Si close to the band-gap (λ ∼1120 nm). Due to the parasitically absorbing back contact, most of the light that goes into the cell is absorbed. Therefore, bare$_A$ reduces only slightly in this wavelength range.

Optics EXPRESS

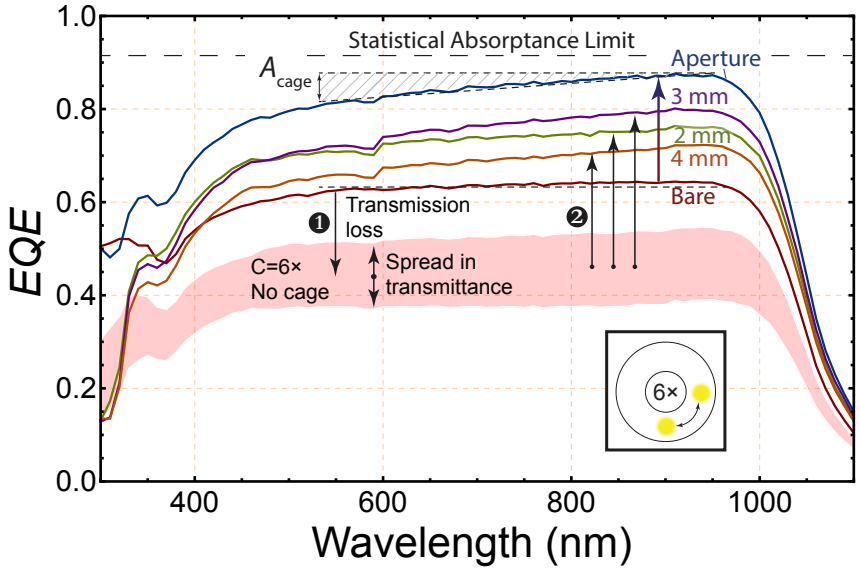

Fig. 5. Plot of the EQE for different cage heights measured using the $C = 6\times$ concentrator. The red line shows the EQE of the bare solar cell, which has a plateau at 0.64 (see bottom dashed line). The light-red shaded area indicates the drop in EQE when the concentrator is placed directly on top of the cell due to parasitic absorption in the concentrator (182). The integration of a cage below the concentrator results in external light trapping. Thereby, the EQE of cell with external light trap exceeds the EQE of the bare cell (see 183). The upper blue line (EQE_{aperture}) shows the EQE for a slightly tilted beam of light that passed the aperture without hitting the concentrator, for a cage height of 4 mm. EQE_{aperture} closely approximates the black dashed statistical absorptance limit for a cell with a reflectance of 36%. The inset shows the top view of the concentrator and roughly indicates the size of the monochromatic beam.

To measure the spectral response of the cell in the presence of a light trap, a 4 mm tall cage was placed on top of the solar cell, onto which a concentrator with different concentration factors (C=3×, 6×, or 9×) was mounted. It was found that the optical transmittance of each concentrator varies significantly with the location of the incident (collimated) beam (diameter ∼2.5 mm), as we show later. The reported EQE are the best measured data of the same cell (with and without light trap). A significant broadband enhancement of the EQE is observed for all configurations of the light trap. The trap with a 6× and 9× concentrator show higher improvement than the trap with a 3× concentrator due to enhanced external light trapping. The analytical model and the simulations explain how the concentration factor affects the EQE and absorptance.

The absorptance of a solar cell with an external light trap on top (A_{trap}) cannot be easily measured. However, it can be extracted from the EQE and the internal quantum efficiency ($IQE = \frac{EQE_{\text{bare}}}{A_{\text{bare}}}$) according to:

$$A_{\text{trap}} = \frac{EQE_{\text{trap}}}{IQE} = \frac{EQE_{\text{trap}}}{EQE_{\text{bare}}} \cdot A_{\text{bare}}. \tag{1}$$

Using this formula we calculated the absorptance of the 9× concentrator ($9\times_A$, dashed blue line). It can be seen that the overall absorptance improved by almost $20\%_{\text{abs}}$.

The transmittance of a concentrator is linearly related to the EQE of the cell in the presence of the external light trap and is determined by the reflectivity of the silver surface (Ag_R). The gray dashed curve shows the measured reflectivity of a flat, polished part of silver over-coated

Optics EXPRESS

aluminum. The strong decrease in the EQE around ∼310 nm (see arrow) is due to parasitic absorptance in the silver. This corresponds to our earlier observations [31] and does not represent a large absolute loss since there is only a small number of photons in this range of the solar spectrum.

***EQE* for several cage heights**. In the external light trap a fraction of the reflected photons is reflected back to the solar cell by the reflective bottom of the concentrator. The size of this fraction is partly determined by the cage height. When the concentrator is placed directly on top of the solar cell (so there is no cage) there is no light trapping. Due to the parasitic absorptance by the concentrator the absorptance in the cell drops. Upon insertion of a (sufficiently tall) cage, a fraction of the reflected light is recycled. Therefore, by changing the cage height, the optical recycling efficiency is altered. We measured the wavelength dependent cell response for several trap configurations with different cage height (Fig. 5).

First, a concentrator with $C = 6\times$ is placed directly above the solar cell. The EQE drops due to the non-unity transmittance of the concentrator as a result of parasitic absorptance in the silver. There is a spread in the data due to the spatial variation in the transmittance of the concentrator.

The EQE improves significantly when a cage is inserted between the concentrator and the solar cell. The best measured EQE for a 2, 3, and 4 mm high cage are shown in green, purple, and orange respectively. A broadband EQE enhancement over the entire spectral range is observed. The EQE decreased for wavelengths shorter than ∼350 nm (as was also observed in Fig 4). Due to the strong variations in the transmittance of the concentrator for different positions of the illumination spot, we cannot determine a clear relation between the EQE and the cage height.

Potential. To indicate the potential improvement of the EQE when the concentrator has unity transmittance, we positioned the beam under a small angle, directly through the aperture without the light hitting the concentrator. The corresponding EQE is shown as the blue curve. This illustrates the potential for an ultimate external light trap. The EQE improved from ∼64% to ∼88% (=+38%$_{\text{rel}}$). The reflectance of the cell was reduced from ∼36% to 12%. Later in this paper, a statistical model is introduced which gives a statistical absorptance limit (Eq. (3)). The limit for this trap configuration is an absorptance of 91.4% ($R = 8.6\%$), which is close to the experimentally observed absorptance of ∼88%. A similar reduction in reflectance can be expected for a thin, planar cell with an anti-reflection coating.

Comparing EQE_{bare} and EQE_{aperture}, it is notable that EQE_{bare} has a horizontal plateau, while EQE_{aperture} has a slope (see both dashed lines). For a perfect light trap (in which all wavelengths are retro-reflected with equal reflectivity) the EQE improvement should not be wavelength dependent. The small improvement from ∼600 nm onwards is due to *decreasing* parasitic absorptance (with increase of wavelength) in the silver coating of the cage (indicated A_{cage}).

3.1. Transmittance of the parabolic concentrators

The performance of an external light trap is proportional to the transmittance of the concentrator [32]. We measured the transmittance of the concentrators and compared it to the theoretical transmittance calculated from the optical constants of silver. The optical constants (n and κ) of a freshly sputtered silver layer on a flat glass plate were determined by spectroscopic ellipsometry. We calculated the spectral reflectance using the Fresnel equations with the measured n and κ. Figure 6(a) shows the calculated reflectance at a wavelength of 532 nm as a function the angle of incidence (θ_i) for different polarizations. The reflectance of such a flat layer is ∼96-100%, and is highest for s-polarized light. Based on these reflectance values and the curvature of the concentrator we calculated the transmittance of each position of the concentrator.

We also measured the spatially resolved transmittance of the concentrators by raster scanning the illumination position of a collimated laser beam over the surface of the concentrator. An optical single mode polarization-maintaining optical fiber is connected to the laser and is

Optics EXPRESS

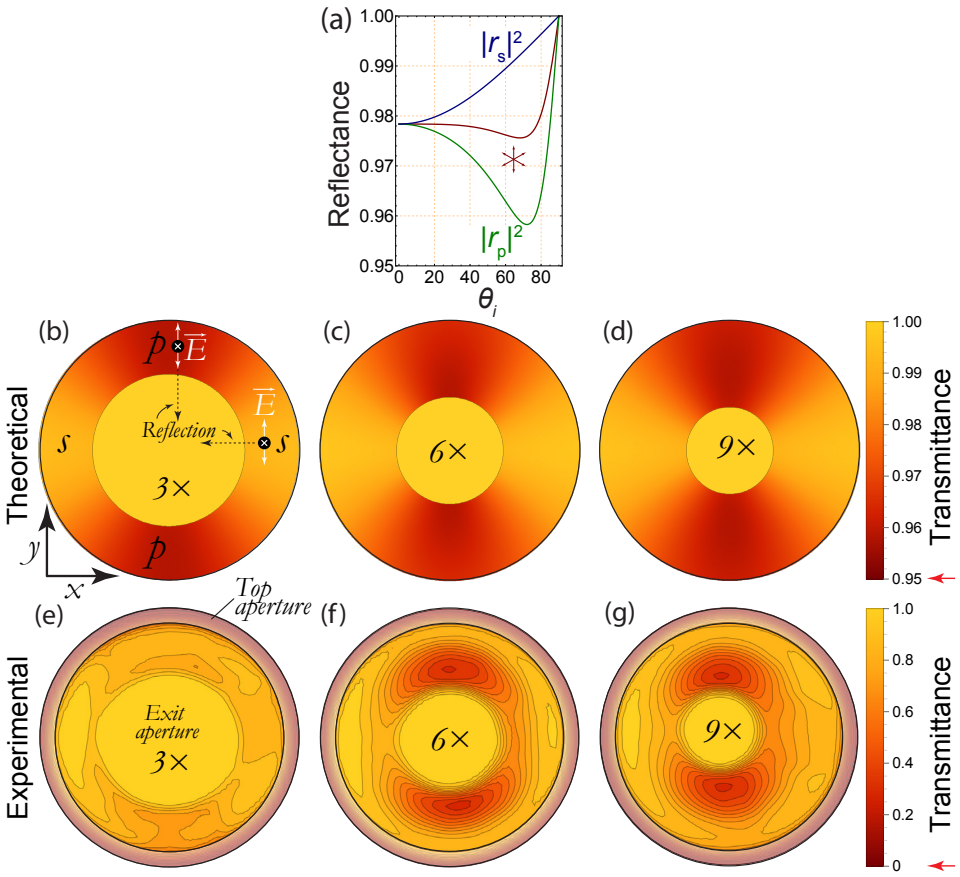

Fig. 6. Comparison of the theoretical and experimental transmittance of the concentrators. **(a)** Reflectance as a function of the angle of incidence (θ_i) of a smooth silver surface, for *s*-, *p*-, and un-polarized ($*$) light, at a wavelength of 532 nm. This data is used to calculate the following transmittance maps. (**b-d**) Calculated transmittance maps according to the Fresnel equations based on the polarization and incidence angle of the three silver coated concentrators (C=3×, 6×, and 9×) for incoming light (532 nm), traveling parallel to the concentrator axis. The maps (top view of concentrator) show the transmittance as a function of the incidence (x, y) position. Due to the geometry of the concentrator, the light can be *p*-polarized and *s*polarized with respect to the plane of incidence depending on the incident spot. (**e-g**) Experimental transmittance maps for light with a wavelength of 532 nm. Note that the color bars of the theoretical and experimental maps differ significantly. The measured transmittance at the outer edge is faded out, to indicate that the laser beam slightly overlaps with the rim of the concentrator.

Optics EXPRESS

fixed to a 2D-automated stage. The concentrator is mounted in front of an integrating sphere with a photodiode. The integrating sphere distributes the total transmittance such that the photodetector is homogeneously illuminated, without collecting any direct reflection. The spot size of the 532 nm diode laser is less than 1 mm. The beam propagates parallel to the central concentrator axis.

Figure 6 shows the calculated (Figs. 6(b)-6(d)) and measured (Figs. 6(e)-6(g)) transmittance maps of the concentrators for polarized light. Light traveling through the center of the concentrator is fully transmitted. Light hitting the concentrator is reflected once before it reaches the bottom aperture. The transmittance was calculated using the calculated Fresnel reflection coefficients, see Fig. 6(a). A notable difference between the reflections of the two polarization directions is observed. The light at the top and bottom of the concentrator is *p*-polarized, while at the left and right side it is *s*-polarized, which gives rise to a lower transmittance for light incident on the top and bottom part of the concentrator.

Figures 6(e)- 6(g) show the measured transmittance of the parabolic mirrors, which is significantly lower than the values based on theoretical Fresnel reflection (note the different colorbar range). The 3× concentrator has higher transmittance (74-93%) than the 6×, and 9× concentrator (31-93%). Especially the transmittance of *p*-polarized light is significantly lower than expected. We analyze the origin of this reduced transmittance in the next section.

3.2. Surface quality of the concentrators

The track of the milling cutter leaves small grooves on the surface of the concentrator. Figure 7(a) shows a schematic top view of the 6× concentrator and it illustrates the milling tracks. The size of these scratches is determined by the material hardness and several settings of the milling machine, like the overlap between consecutive drill paths and the shape and size of the milling cutter.

The reflectivity and surface quality of the concentrator surface affects its transmittance. By visual inspection of the concentrator surface some haze is observed, which indicates scattering due to surface imperfections. Due to the strong curvature of the surface it is not possible to scan the surface by conventional AFM and surface profilers. However, we can get an indication of the surface roughness from SEM images.

Figures 7(b)-7(d) show several SEM images of the surface. Figure 7(b) shows a milled concentrator directly after fabrication. The milling lines can be clearly observed. The deposition of silver slightly improves the surface quality, but still some artifacts remain, as shown in Fig. 7(b). The visible metal blobs have a feature size in the order of microns. After silver deposition on these rough blobs, small silver grains are observed. There are thus different origins of surface roughness with each a typical feature size. Although the surface roughness cannot be quantified based on this images, we do observe that typical feature sizes in the order of hundred nanometers. This is the origin of the observed reduced transmittance. We conclude that the current fabrication method has to be improved to meet the requirements for external light trapping. Nevertheless, these initial experiments already improve our understanding of potential issues. Smoother surfaces can be obtained by diamond turning on a lathe or a better smoothening procedure. Also, the use of dielectric CPC with an ARC can have an excellent broadband reflectance less than 0.5% [33]. These CPCs can be fabricated by a process called ultra-precision glass pressing.

4. Modeling & theory

To obtain a detailed understanding of the effect of the concentration factor and cage height on the absorptance by the solar cell, we introduce a generic analytic model based on statistical ray optics. We compare the results of this statistical model with the results obtained by ray tracing. The ray tracing also gives detailed understanding of the effect of the cage height and

Optics EXPRESS

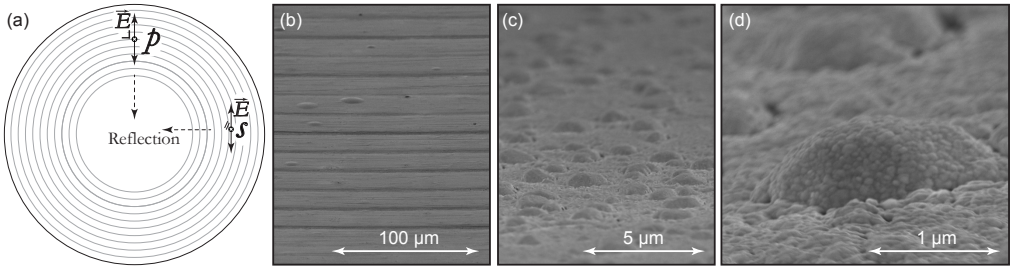

Fig. 7. **(a)** Schematic top view of a concentrator. The concentric circles illustrate a few milling lines. Polarized light hitting the concentrator induces oscillating electrical currents on the surface of the concentrator. At the top and bottom these currents are orthogonal to the milled circles, while at the left and right side these currents are parallel to the milled lines. This difference in orientation has a major impact on the observed reflectance. **(b-d)** SEM images of the concentrator surface. (**b**) A 3× aluminum concentrator before deposition of silver. The regular stripes are caused by the milling process. **(c)** A 6× concentrator after polishing and evaporation of Ag. **(d)** Zoom-in of a metal blob on which different metal grains can be seen.

concentration factor on the cell illumination.

4.1. Statistical model with Lambertian scattering

In this statistical model we first determine the probability for a photon that is inside the reflective cage to escape via the aperture. After determining this escape probability we can calculate a well-defined statistically averaged absorptance for the overwhelmingly large ensemble of photons in the solar spectrum. An upwards moving photon in the cage with an arbitrary position and orientation has an escape probability (P_{escape}) which is given by the following area ratio:

$$P_{\text{escape}} = \frac{A_{\text{aperture}}}{A_{\text{concentrator}}} (= \frac{1}{C}). \tag{2}$$

This statistical assumption is for example valid for isotropically distributed light in an integrating sphere, but is not necessarily true for other trap geometries such as our trap [37]. For Eq. (2) to be true for our external light trap, it has to be proven that there is a well-defined statistical escape probability for the ensemble of upward moving photons. This escape condition is for example also fulfilled when the light intensity is homogenized when it reaches the aperture plane after being reflected by the solar cell. The cage height is one of the parameters that determines the degree of this homogeneity and thereby the accuracy of the following analytical model.

If the statistic condition for Eq. (2) is fulfilled then the (integrated) absorptance (A_{t}) of the solar cell with a light trap is given by [31,32]:

$$A_{\text{t}} = T_{\text{c}} \cdot \frac{A_{\text{sc}}}{1 - R_{\text{sc}}(1 - C^{-1})R_{\text{cage}}}, \tag{3}$$

with T_c the transmittance of the parabolic mirror, A_{sc} the absorptance of the solar cell and R_{cage} the reflectance of the top of the cage (the reflectance of the four sides is assumed to be 1).

This model is valid for incoming light within the acceptance angle. The acceptance angle determines the amount of diffuse light that can enter the cage. The optimal value for C is therefore a trade-off between the degree of light trapping and the acceptance of light. From this statistical model we can determine the following two limits.

In the limit of high cell absorptance (A_{sc} ~0.8-1) it can be seen (e.g. by making a Taylor series) that the reflectance of the cell with trap (R_{t}) reduces according to $R_{\text{t}} \sim \frac{R_{\text{sc}}}{C}$. As a rule of thumb, the effective reflectance of modules with a trap is thus reduced by a factor C.

Optics EXPRESS

For specular reflection of light, the entropy is preserved. Interestingly, it has been shown that the escape probability can be reduced below the statistical escape probability of randomized light by deterministic light trapping [39], thereby the $4n^2$ internal path length enhancement limit can be surpassed. Due to the conservation of etendue and entropy upon specular reflection in the external light trap there are certain cases in which the statistical absorptance limit is exceeded.

From a thermodynamic point of view, the effective emitting area of a cage with a small aperture is reduced to only the aperture area. The radiation coming from the aperture equals that of a (perfect) black body with an emissivity of 1 as shown by Planck [40]. Here, it is assumed that the walls do not transmit any radiation to the exterior. Due to reciprocity, the effective absorptivity of light entering the cage via aperture is thus 1. Thereby, the thermodynamic energy conversion efficiency limit of this system is higher than that of bare solar cells [41]. For a cell in an external light trap this elevated efficiency limit is caused by a net reduction of the radiative recombination current due to recycling which results in a larger splitting of the quasi Fermi-levels and thus a higher V_{oc}.

4.2. Ray tracing of external light trap & effect of cage height

The conditions for the statistical model are not necessarily satisfied for all configurations of the external light trap. To analyze the effect of the cage height and the concentration factor on the cell absorptance and spatial intensity distribution on the cell, we set up a series of light traps with different cage height and performed ray tracing using *LightTools*, a non-sequential ray-tracer software package from *Synopsys*. The setup is illustrated in Fig. 8(a). A collimated beam of light, consisting of 1 million rays, is directed to a $C = 6\times$ reflective compound parabolic concentrator (CPC) [42], which funnels the rays through a small aperture, via a perfectly specular reflective cage, towards the solar cell. The response of this setup is equivalent to the response of a module with a large array of external light traps, without any 'vertical' walls. The simulation of a ray continues until the ray escapes out of the concentrator or until the energy of the ray dropped to less than 1% of its initial energy.

Figure 8(b) shows the total absorptance in the solar cell, as a function of the cage height for two reflectance levels. The reflectance of 36% represents the overall reflectance of our cell, and 13% represents that of a typical industrial solar module. For a very short cage ($h_{cage} < 1\,mm$), the light is concentrated on a small spot in the center of the cell and the reflected light will escape. Once the cage becomes higher than $\sim 1\,mm$ there is a sudden increase in the absorptance as an increasing amount of light retro-reflected by the top of the cage just next to the aperture. This fraction steadily increases up to $h_{cage} \sim 6\,mm$. There is an optimum absorptance around this cage height because the escape probability at this cage height is low (so high recycling efficiency) during the first couple of recycling events. These first recycle events are most important as the (reflected) intensity is highest at these instances [32, 39].

When a light trap with a 6 mm cage is applied on our solar cell (with $R = 36\%$) the reflectance at normal incidence is reduced to 12%; for a typical industrial solar module the reflectance drops from 13% to 4%. At normal incidence the light that reflects from the center of the cell is not trapped; it escapes directly through the aperture. At other angles of incidence, this "central light" can be totally retro-reflected to the cell. Interestingly, the statistical absorptance limit is exceeded in these cases because the escape probability of photons becomes lower than the area fraction of the aperture.

Interestingly, the statistical absorptance limit is exceeded in these cases, because the escape probability of photons becomes lower than the statistical escape probability as given by Eq. (2).

The dashed lines indicate the statistical limit calculated using Eq. (3) at $C = 6\times$. For $R = 36\%$ and $R = 13\%$ the reflectance is reduced to 8.6% and 2.4% respectively. The derived reflection reduction of $R_t \sim \frac{R_{sc}}{C}$ yields $R_t = 2.1$ for $R = 13\%$, so this is a reasonable approximation. For larger cage heights ($h_{cage} > 6\,mm$) and normal incidence, the light distribution becomes more

Optics EXPRESS

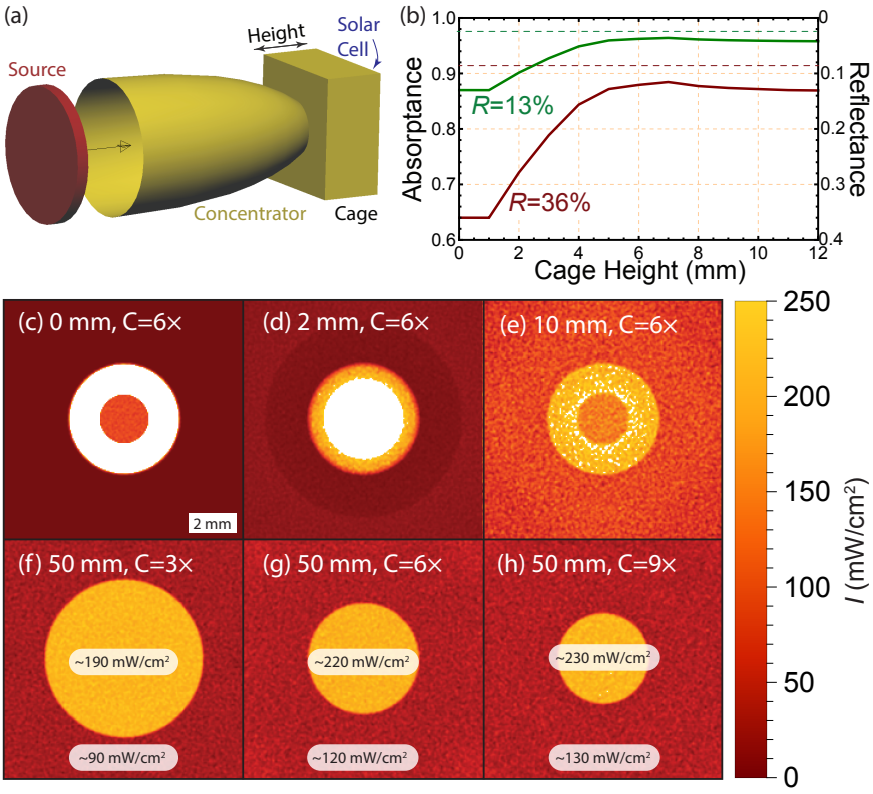

Fig. 8. (**a**) Illustration of the setup used for the ray tracing. A light source with a collimated beam is aimed at the $C = 6\times$ concentrator with a cage and solar cell behind. A series of simulations was performed with different cage height. The simulations are performed at normal incidence. **(b)** Effective absorptance by a cell within an external light trap with $C = 6\times$. The reflectivity represents that of our cell (36%) and that of a typical solar module (13%). For a short cage the light is not trapped. The absorptance increases initially, and levels off at ~6 mm. The dashed lines show the statistical absorptance limit. (**c-e**) Simulated intensity distribution on the solar cell with increase of cage height (0−10 mm) for $R = 36\%$, and $C = 6\times$. The absorptance becomes more homogeneous with increase of the cage height. For pixels with a white color the absorptance exceeds 250 mW/cm^2. (**f-h**) Intensity maps for $h_{\text{cage}} = 50$ mm, $R = 36\%$ at $C = 3\times$, $6\times$, and $9\times$. The central ring is illuminated stronger due to direct and reflected illumination.

Optics EXPRESS

and more homogeneous. Thereby, the absorptance determined by the ray tracing approximates that of the statistical limit (dashed line) within a few percent. The small absorptance difference between the ray tracing and analytical model is caused by the direct escape of the specular reflection of the center of the cell. This fraction ($R_{sc} \cdot 1/C$) is thus not trapped at normal incidence. At different incoming angles, the direct reflection of the cell can be completely reflected, and thereby the statistical limit is surpassed. Averaged over all incoming angles (θ_i) within the acceptance angle of the CPC, the escape probability is only defined by the ratio $A_{aperture}/A_{sc}$, and A_t is therefore given by the statistical limit (see Eq. (3)). The statistical model thus gives an excellent approximation of the absorptance of a cell with an external light trap.

Figures 8(c)-8(e), and 8(g) show the intensity distribution on the cell for different cage heights ($h_{cage} = 0 - 50$ mm) at $C = 6\times$. In absence of a cage (h_{cage}=0, Fig. 8(c)), the center is illuminated by $\sim 6\times$ concentrated light. For a 2 mm cage, see for example Fig. 8(d), most of the light hits the cell and is reflected without being trapped and the cell illumination is still rather inhomogeneous. The rays enter the cage with a distribution of propagation angles. Therefore, the spread of the beam becomes more and more homogeneous as light travels through the cage. For taller cages, for example those in Fig. 8(e) and 8(g), most of the reflected light gets trapped; most of the reflected light hits the top of the cage and is reflected back to the cell. The circular white spot in the center is caused by the light that went straight through the aperture (without being reflected by the CPC). Due to the divergence of the beam after the CPC and the light trapping the illumination of the outer area of the solar cell is very homogeneous.

Spatial intensity distribution and cell response. Figures 8(f)-8(h) show the intensity distribution for a tall cage at $C = 3\times, 6\times$, and $9\times$. The cage height determines the intensity distribution on the cell. The intensity of the light source is $100\,\mathrm{mW/cm^2}$. It can be seen that the cell on average operates at a higher irradiance level due to the light trapping. For a tall cage, the light distributes homogeneously over the cell, except on the center. The intensity in the center of the solar cell is roughly twice as high as the outer area. Inhomogeneous cell illumination can be detrimental for the cell response because of Ohmic losses and local heating [28, 43]. Mild intensity fluctuations do not impact the performance of most solar cells as long as the maximum-to-average intensity ratio is less than ~ 3 [28]. The observed intensity difference of a factor ~ 2 is therefore acceptable. If improved homogeneity is needed this can be realized by integrating a diffuser in the cage. By downsizing the dimensions of the external light trap to $\sim 100\,\mu$m (order of magnitude of the thickness of the solar cell) the impact of inhomogeneity can be further reduced as the electrical current will redistributed evenly over the cell after a short ($\sim 100\ \mu$m) lateral distance. If needed, the light can be more randomized by using a secondary optical component, such as a prism, or diffuser at the exit of the concentrator.

For large area application of external light trapping it is practical to use a matrix of concentrators. Circular symmetric parabolic mirrors are unable to provide low area losses due to imperfect filling fraction. To minimize area losses we previously [31] showed how square, hexagonal, or vertically truncated concentrators can be used to reduce the area losses to an arbitrarily low number. A dead area loss of 1% is feasible with these designs and the effectiveness of the external light trap would be retained within a concentrator array.

4.3. *Incoupling of diffuse light by external light trapping*

An inevitable consequence of external light trapping is the restriction of incoming photons from certain angles. Photons entering the concentrator from an angle larger than the acceptance angle are reflected backwards by the concentrator. This reduces the power output of the module. However, this problem can be solved by geometrical separation of the diffuse and direct light, after which both components are sent so a separate cell [44].

Tracking the sun enables complete incoupling of the direct component of the sunlight. However, as tracking results in higher costs, it can be beneficial to use a static module, which captures

Optics EXPRESS

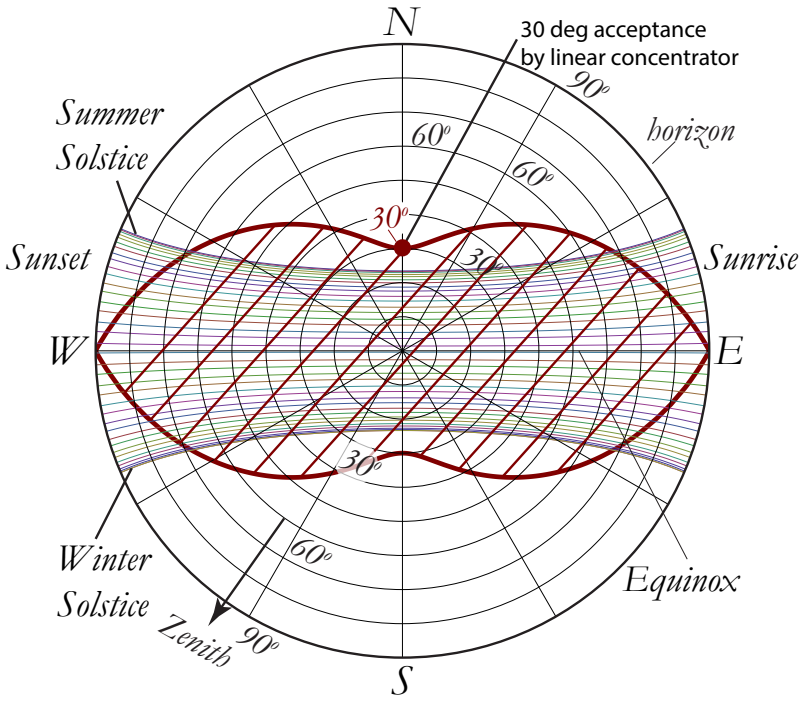

Fig. 9. Polar plot of the path of the sun during one year for a location on the equator. The concentric rings indicate the elevation of the sun and the position on the ring is the compass direction. If the sun is directly overhead it is in the center of this plot. During the summer and winter solstice, the sun moves along the top and bottom curve respectively. The red line shows the boundary of the acceptance angles for a static, horizontal module with a linear concentrator.

most of the direct sunlight [45]. This can be realized quite well by a linear concentrator that is oriented along the East-West direction. Figure 9 shows a polar plot with the yearly path of the sun, as seen from a location on the equator. The red line shows the outer boundary of the geometric acceptance area for a horizontal module with a linear CPC. The acceptance angle of the CPC is 30°, which corresponds to $C = 2\times$ for a hollow concentrator. Due to the axial tilt of the earth the path of the sun varies during the year. The tilt of the earth axis is $\sim 23°$. Therefore, this is the elevation angle at noon during summer and winters solstice. By using an acceptance angle that is larger than this tilt angle the sunlight can still be collected most of the day. The border of the acceptance area of a linear concentrator with an acceptance angle of 30° is marked by the red line. As this acceptance angle is larger than the tilt of earth axis, all light is accepted during noon (sun on direct North or South). During the equinox (sun on East-West line), the direct light of the sun is accepted from sunrise (east) to sunset (west). For other days of the year there is a small cut-off just after sunrise and just before sunset. However, this is only a small fraction of the daytime and moreover, the intensity at low elevation (sun close to horizon) on the solar module is low due to the cosines projection area factor and the longer path length through the atmosphere. The projected area [6] of a module decreases according to $I = I_{\text{sun}} \cdot \cos(\text{elevation})$. Alternatively, micro-trackers form an interesting alternative that does not require to tilt the complete module [46].

Optics EXPRESS

5. Conclusions

We explored the potential of an external light trapping as a universal solution for light management on module level. We showed enhanced EQE of a prototype crystalline silicon photodiode due to optical confinement by an external light trap over the full solar spectrum. The light trap can be effective for all types of solar cells, in particular for thin multi-crystalline Si cells that are difficult to texture and thin-film cells which have low-index absorber layers for which internal light trapping is less effective. Using our thick prototype c-Si solar cell without an AR coating, our proof-of-principle c-Si photodiode showed an absorptance enhancement from 64 to 87% by external light trapping. The parasitic absorptance in the experimental prototype concentrators is much higher than expected. The associated transmittance is too low to improve the performance of thick, conventional solar cells. It shows that concentrator transmittance is crucial in this light trapping concept. A concentrator transmittance in the range of 95-100% is required to improve the performance of such cells. Dielectric CPCs with a transmittance of more than 99.5% can be very suitable [33]. The reflection reduction of a factor $\sim$3 can also be expected for very thin c-Si solar cells when concentrators with higher transmittance are used. We compared the results of our statistical model and that of ray tracing for our trap design. It was found that the model gives a good approximation of the total absorptance. Our optical model shows that on module level a reflectance reduction from 13% to 2.4% is feasible. Our simulations show improved absorptance and homogeneity of the cell illumination with increase of cage height. We found that there can be a factor two difference in intensity on cell level due to the external light trap. This intensity distribution is acceptable since such an intensity contrast does not reduce the cell performance significantly [28, 43]. It was shown that sun tracking is not required for this system if the acceptance area of the concentrator is matched to the path of the sun.

Imperfections of the concentrator surface were found to result in strong polarization-dependent transmittance. The milling process needs to be improved to meet the transmittance requirements for module application. Alternatively, there are many other lens fabrication technologies, like diamond turning and ultra-precision glass pressing, that offer higher surface quality and thereby major improvements to the concentrator transmittance.

Due to external light trapping, the cell thickness can be reduced by a factor of at least 2, without reducing absorptance. The use of an external light trap with thin, planar c-Si cells does not only result in higher short circuit currents, but also in increased V_{oc} due to reduced bulk and surface recombination.

We explored the potential of external light trapping as a simple and effective overall light management solution. As the trap enables further thinning down of c-Si solar cells and as it is capable to simultaneously recycle the various broadband reflection sources on the module level, it deserves serious attention as a candidate for highly-efficient solar modules of the foreseeable future.

Acknowledgments

The authors acknowledge the insightful discussions with and the help of A. Polman, Z. Krumer, N.J. Bakker, K Sinapis, A. Parretta, D.K.G. de Boer, H. Boluijt, D.J. Spaanderman, and M. Borsboom. We acknowledge Synopsys for the educational license of LightTools. This work is supported by NanoNextNL of the Government of the Netherlands and 130 partners.

194.171.111.64 {ts '2016-10-05 04:24:34'}